First-principles study of fission product (Xe, Cs, Sr) incorporation and segregation in alkaline earth metal oxides, HfO_2, and the MgO–HfO_2 interface

2009 J. Phys.: Condens. Matter 21 045403

(http://iopscience.iop.org/0953-8984/21/4/045403)

J. Phys.: Condens. Matter **21** (2009) 045403 (7pp) doi:10.1088/0953-8984/21/4/045403

First-principles study of fission product (Xe, Cs, Sr) incorporation and segregation in alkaline earth metal oxides, HfO_2, and the MgO–HfO_2 interface

Xiang-Yang Liu, Blas P Uberuaga and Kurt E Sickafus

Materials Science and Technology Division, Los Alamos National Laboratory, Los Alamos, NM 87545, USA

Received 7 October 2008, in final form 26 November 2008
Published 8 January 2009
Online at stacks.iop.org/JPhysCM/21/045403

Abstract

In order to close the nuclear fuel cycle, advanced concepts for separating out fission products are necessary. One approach is to use a dispersion fuel form in which a fissile core is surrounded by an inert matrix that captures and immobilizes the fission products from the core. If this inert matrix can be easily separated from the fuel, via e.g. solution chemistry, the fission products can be separated from the fissile material. We examine a surrogate dispersion fuel composition, in which hafnia (HfO_2) is a surrogate for the fissile core and alkaline earth metal oxides are used as the inert matrix. The questions of fission product incorporation in these oxides and possible segregation behavior at interfaces are considered. Density functional theory based calculations for fission product elements (Xe, Sr, and Cs) in these oxides are carried out. We find smaller incorporation energy in hafnia than in MgO for Cs and Sr, and Xe if variation of charge state is allowed. We also find that this trend is reversed or reduced for alkaline earth metal oxides with large cation sizes. Model interfacial calculations show a strong tendency of segregation from bulk MgO to MgO–HfO_2 interfaces.

(Some figures in this article are in colour only in the electronic version)

1. Introduction

In order to close the nuclear fuel cycle, advanced concepts for separating out fission products are necessary. One method for doing this is a dispersion fuel form in which a fissile core is surrounded by an inert matrix that captures and immobilizes the fission products from the core. If this inert matrix can be easily separated from the fuel, via e.g. solution chemistry, the fission products can be separated from the fissile core. Possible inert matrix materials include alkaline earth metal oxides. The fissile core is composed of an actinide-bearing material, and UO_2 is an obvious choice for the core. A surrogate material, studied due to experimental convenience, for the fissile core is HfO_2. One important question in such a dispersion fuel form is the segregation behavior between the different bulk phases and the interface between the matrix and fuel core. In this paper, we use density functional theory (DFT) based first-principles method to study the incorporation and segregation of a selection of important fission products in alkaline earth metal oxides, HfO_2, and the MgO–HfO_2 interface. The present study deals with three fission products: Xe, Cs, and Sr, which are all abundant in spent nuclear fuels. Sr is considered as a tracer for spent fuel dissolution [1]. Both Cs and Sr are relatively hot in spent fuels so it is strongly advantageous to separate these elements out.

The alkaline earth metal oxides considered in this work include MgO, CaO, SrO, and BaO, which each has the rock-salt structure. HfO_2 exists in three forms: monoclinic, tetragonal (>2000 K), and cubic fluorite (CaF_2) (>2870 K), which all have the same ionic bonding and are structurally closely related. The lower symmetry monoclinic phase is most stable, and usually found in experimental studies. However, the cubic phase is simplest to treat computationally and for structural models [2]. Since we are interested in modeling hafnia as a surrogate material for oxide fuels such as UO_2, the cubic fluorite structure for hafnia is used in this work. We evaluate the thermodynamic enthalpies from total energy calculations; entropy effects are ignored.

Previous theoretical work includes atomistic simulations of noble gas incorporation in minerals using empirical potentials of the Buckingham form [3]. In that study, the incorporation of noble gases Ne, Ar, Kr, and Xe in a variety of minerals including MgO, CaO, diopside, and forsterite was studied. For MgO, a Mg lattice site was found to be more favorable than an interstitial position for all the noble gases studied. For CaO, heavy noble gases such as Xe also prefer to substitute on the Ca lattice site. It should be noted that in that study, defect complexes such as Schottky defects (stoichiometric or different charged pairs of vacancies) were not considered. However, we demonstrate in this study that defect complexes such as Schottky defects are preferred defect sites for fission product incorporation.

2. Methods

The DFT based plane-wave code Vienna *Ab initio* Simulation Package (VASP) [4] was used for our calculations. The generalized gradient approximation (GGA) was used for the exchange correlation potential, with the functional of Perdew–Wang 91 (PW-91). Projector-augmented wave (PAW) pseudopotentials were employed. For the elements comprising the oxide structures, the valence electron configurations in the PAW pseudopotentials are $2s^2 2p^4$ for O, $3s^2$ for Mg, $3p^6 4s^2$ for Ca, $4s^2 4p^6 5s^2$ for Sr, $5s^2 5p^6 6s^2$ for Ba, and $5p^6 5d^2 6s^2$ for Hf. For fission products, the valence electron configurations are $5s^2 5p^6$ for Xe, $5s^2 5p^6 6s^1$ for Cs, and $4s^2 4p^6 5s^2$ for Sr. A plane-wave basis set with an energy cutoff of 250 eV was used. This cutoff was used in a previous study of MgO addimer diffusion on MgO(100) surface [5] and found to be appropriate for PAW pseudopotentials.

For the defect-free bulk calculations, a unit cell of 8 atoms was used for alkaline earth metal oxides, and a unit cell of 12 atoms used for HfO_2. 6^3 Monkhorst–Pack (MP) k-point sampling was used. For defect calculations, a $2\times2\times2$ supercell was used with 64 atoms for alkaline earth metal oxides and 96 atoms for HfO_2. 2^3 MP k-point sampling was used in these cases. An equivalent k-point sampling was also used in the interface calculations. A force-relaxation criterion of 0.2 eV $Å^{-1}$ was used in the bulk defect calculations, yielding energy convergence error estimated to be around 0.2 eV or less. For interface calculations, a force-relaxation criterion of 0.05 eV $Å^{-1}$ was used. Electronic states were occupied according to a Gaussian distribution with a smearing width of 0.05 eV.

Besides the complex defects that must be considered (e.g., Schottky defects, Frenkel defects, and defect clusters [6]), one complicated issue in modeling defects in oxides is the possibility of multiple-charge states associated with defects. There are two theoretical approaches to studying defect energetics in oxides in literature, and we will consider a third:

(1) *Neutral defects*. In one approach that is typical of DFT studies, only the energies of non-charged defects are calculated or defects energies in various possible charge states are calculated but not compared to each other [7]. Here the neutral defects are defined as defects with no net charge.

(2) *Full charge compensation model*. In this approach, a charge compensation model is used in which the atoms comprising defects are assumed to be in their most probable ionic charge states, as defined by their charge state in perfect bulk. In this approach, in order to take into account the ionic nature of the material, only the core is modeled for cations while for anions such as oxygen, an O core together with eight electrons is modeled. That is, full charge transfer between cations and anions is assumed. For example, an oxygen vacancy is always modeled as V_O^{2+}. This approach, widely used in empirical potential calculations, has now also been adopted in several DFT studies [8–11]. In this work, we compare the results of both approaches (1) and (2) for some typical defects in MgO.

(3) *Variable charge model*. Finally, we consider a third alternative. For the first time, we determine the lowest energy charge state for each defect individually. That is, each defect is allowed to assume the charge state which minimizes its energy, regardless of the charge state other defects might assume. This analysis is applicable to point defects. In the case of clustered defects, such as the Schottky defect, where charge neutrality is maintained, such considerations are not necessary.

For calculations of charged supercells, a neutralizing background charge was imposed automatically in the VASP calculations. The formation energy of a defect in the supercell can be expressed as,

$$E^{\mathrm{f}} = E_{\mathrm{tot}} - E_{\mathrm{bulk}} - \mu + q(E_{\mathrm{F}} + E_{\mathrm{v}}) \qquad (1)$$

E_{tot} is the total energy of the supercell with defect, and E_{bulk} is energy of the undefected bulk system. μ is the chemical potential, representing the reservoirs with which atoms are exchanged. E_{F} is the Fermi level, referenced to the valence band maximum in the bulk. We set E_{F} to zero, meaning that the details of the Fermi level effect not treated. E_{v} is the energy of the valence band maximum in the defect state.

Our calculations are performed within periodic supercells. In the case of charged cells, the point charge q at the defect and the neutralizing jelly $-q$ interact not only within the cell, but also across different periodic replicas of the cell, similar to the infinite-range interactions in an ionic crystal. To correct for this artifact of the periodic boundary conditions, we apply the monopole correction of $e^2q^2\alpha/(L\epsilon)$ (α is the Madelung constant, L the lattice constant of the cubic supercell, and ϵ is the dielectric constant) to the charged systems which increases the total energy for charged systems. Such a correction was originally discussed by Leslie and Gillan [12] and found to yield satisfactory results for supercell calculations of defects in ionic crystals.

3. Results

3.1. Fission product incorporation in bulk oxides

3.1.1. Bulk oxide properties. Bulk properties of alkaline earth metal oxides (MgO, CaO, SrO, and BaO) and hafnia (HfO_2)

were calculated. In table 1, the DFT calculation results of lattice constants and bulk moduli are listed. The fit to the Murnaghan equation of state is used to determine the optimized DFT lattice constant and bulk modulus. The DFT results are in good agreement with available experimental data for all the oxides considered here. The lattice constants predicted are within 1% error of the experimental values except in the case of BaO (1.8% error). The bulk modulus predicted are within 10% error of the experimental values. These error levels are typical in DFT calculations.

3.1.2. Defects in bulk MgO. We examined the different approaches to describing charge states and the resulting defect energies in bulk MgO. A few DFT studies have been performed previously on defect generation and energetics in simple oxides such as MgO [8–11]. Six types of defects were considered in this study: magnesium and oxygen vacancies, isolated Frenkel pairs (interstitial and vacancy pairs) of both magnesium and oxygen, isolated Schottky defects, and bound Schottky divacancy pairs in nearest-neighbor configurations. We present the DFT results in table 2, in three cases representing different approaches to treating charge state effects. In the neutral case, no charge state was considered. In the charge compensation case, all oxygen atoms were in -2 charge state, and magnesium atoms in $+2$ charge state. In the variable charge case, only the lowest energy defect charge state and its associated defect energies are shown.

The vacancy formation energies are calculated with reference to the chemical potential of the species (equation (1)). The oxygen chemical potential is the binding energy of a neutral oxygen molecule, which has an experimental value of -2.55 eV/atom [18], plus the isolated spin-polarized O atomic contribution [19] (-1.52 eV/atom). The magnesium chemical potential is the binding energy of magnesium metal, -1.5 eV/atom. The choice of chemical potential affects only the absolute value of the formation energy of vacancies but not the relative stability of such defects in different charge states. For Frenkel pair and Schottky defects, the chemical potential does not contribute since the total number of atoms in the supercells containing a defect is either equivalent to that in the perfect bulk supercell or only differ by a stoichiometric MgO unit.

The charge compensation results generally improve quite a bit over the neutral results by minimizing the formation energies of defects. For the oxygen vacancy, the neutral defect induces an occupied gap state about 2.7 eV above the valence band maximum (compare to DFT bandgap ∼5.6 eV, and experimental bandgap 7.8 eV). Bader analysis [20] shows that, as a result of removing a neutral oxygen atom from the bulk, the net charge on a neighboring Mg atom decreases from positive $2e$ to positive $0.46e$. This is because in a formal charge sense, the oxygen vacancy should be $+2$. If it is treated as neutral, there are effectively 2 extra electrons in the system, which then increase the electronic charge on the Mg atoms. Explicit consideration of the charge state lowered the formation energy of this defect by 3.9 eV. For the isolated Schottky defect, the formation energy obtained in the charge state calculation is 6.3 eV, in close agreement with previous DFT calculations (6.9 eV [8, 9], 6.99 eV [10], 5.7 eV [11], all with the local density approximation (LDA)). The neutral calculation gives a much higher number, 9.6 eV. The formation energy of the Schottky defect in a bound divacancy configuration is not affected by the charge state, and is lower than that of the isolated Schottky defect.

Table 1. Lattice constants and bulk moduli, computed from DFT calculations and available experimental data.

Property	Calculated		Experimental
		MgO	
Lattice constant (Å)	4.24		4.21 [13]
Bulk modulus (Mbar)	1.51		1.55 [14]
		CaO	
Lattice constant (Å)	4.82		4.81 [13]
Bulk modulus (Mbar)	1.06		1.07 [15]
		SrO	
Lattice constant (Å)	5.20		5.16 [13]
Bulk modulus (Mbar)	0.85		0.91 [16]
		BaO	
Lattice constant (Å)	5.61		5.51 [13]
Bulk modulus (Mbar)	0.70		0.7 [17]
		Cubic HfO_2	
Lattice constant (Å)	5.07		5.08 [13]
Bulk modulus (Mbar)	2.54	—	

For the neutral oxygen interstitial, the highest level that electrons occupy is at the valence band maximum. The oxygen interstitial grabs about $1.4e$ from neighboring oxygen ions, roughly fulfilling the electron orbital requirement for a strongly ionized oxygen atom. However, when two extra electrons are put into the supercell containing an oxygen interstitial, the highest occupied electron state is a gap state, about 2.6 eV above the valence band maximum. As a result, the formation energy of an oxygen interstitial is also higher in the charged state than in the neutral state, leading to a slightly higher formation energy of oxygen Frenkel pair than in the neutral calculations (see table 2). This demonstrates that charge compensation does not always yield a lower formation energy value. The electronic structure may also play a role. In this particular case, there is a strong preference for the neutral charge state rather than the doubly negative charge state (for the oxygen interstitial). Such a preference also applies to the magnesium vacancy case. Here the formation energy of V_{Mg}^{2-} is about 0.5 eV higher than that of V_{Mg}^{0}.

Finally, the largest difference resulting from the charge compensation is for the magnesium Frenkel pair, for which the formation energy reduces from 19.2 eV in the neutral calculations to 9.8 eV, a nearly -10 eV change. This lowering is due to the energy change of magnesium interstitial from the neutral to $+2$ charge state. For the neutral magnesium interstitial, I_{Mg}^{0}, the highest occupied electron state is at the bottom of the conduction band with two electrons. For $+2$ charge state, I_{Mg}^{2+}, the Fermi level drops to the valence band level, so the total energy is lowered by roughly $2E_{gap}$.

Through defect studies in MgO, we found that the charge compensation model in general yields better energetic results than the neutral calculations. However, for certain cases, point defects can prefer a neutral charge state over a negative charge

Table 2. Formation energies and corresponding charge states of defects in MgO: magnesium and oxygen vacancies (Mg-Vac and O-Vac), magnesium and oxygen Frenkel pairs (Mg-FP and O-FP), isolated Schottky defect (iso-S), and Schottky defect in divacancy configuration (divac-S). Three different sets of results are given: neutral, charge compensation, and variable charge models.

	Mg-Vac	O-Vac	Mg-FP	O-FP	iso-S	divac-S
Neutral model						
Charge state	0	0	0	0	0	0
Formation energies (eV)	8.4	7.8	19.2	12.8	9.6	3.8
Charge compensation model						
Charge state	−2	+2	0	0	0	0
Formation energies (eV)	8.9	3.9	9.8	13.2	6.3	3.8
Variable charge model						
Charge state	0	+2	—	—	—	0
Formation energies (eV)	8.4	3.9	—	—	—	3.8

state, as exemplified by I_O^0 and V_{Mg}^0. In the following, we present calculation results both in the full charge compensation model and variable charge model, in which only the neutral result is used if it is lower in energy than the charged state for a given defect. In this latter case, we are essentially assuming that the excess charge can be transferred to surfaces or grain-boundaries but that locally, the charge can be imbalanced.

3.1.3. Fission product incorporation energies in bulk oxides. From the defect results for MgO, it is clear that, in thermodynamic equilibrium, the dominant defects are Schottky defects, a divacancy pair of Mg and O atoms. This is in agreement with the conclusion from a previous DFT study [11]. In the following, we examine fission product incorporation in bulk oxides, starting with Xe in MgO. The incorporation energy gives the energy required to incorporate a fission product atom at a pre-existing defect site in bulk oxide. Thus, the incorporation energy is defined as,

$$E^{\text{inc}} = E_{\text{tot}} - E_{\text{trap site}} - E_{\text{fission product atom}} \qquad (2)$$

where E_{tot} is the total energy of system with fission product incorporated, $E_{\text{trap site}}$ is the energy of defect system without fission product, and the energy of the fission product atom was calculated as isolated atomic contribution in a cubic supercell with 10 Å in length.

We calculated energies for Xe incorporation at oxygen and magnesium vacancy sites, the interstitial site, and the divacancy Schottky site. The DFT results are listed in table 3. Both results from the charge compensation model and the variable charge calculations are shown in table 3. If not explicitly indicated, the results are from the variable charge calculations. In MgO, the incorporation energy for both Xe_{Mg}^0 and Xe_O^{2+} are higher (by about 3 eV) than that for Xe at a divacancy Schottky site, $(Xe_{Mg}{:}V_O)^0$. The incorporation energy at the interstitial site is even higher (by >10 eV). This indicates that the most favorable configuration for Xe incorporation in MgO is at the bound Schottky site.

In table 3, we also show Xe incorporation energies at the bound Schottky and interstitial sites in other alkaline earth metal oxides CaO, SrO, and BaO, and various defect sites in HfO_2. As in the MgO case, the interstitial sites are quite unfavorable by a large energy difference. However, as cation size increases, the energy required to incorporate Xe in Schottky site decreases.

Table 3. Xenon incorporation energies in bulk oxides. Sites include cation and anion monovacancies (MgO and HfO_2 only), interstitials, nearest-neighbor Schottky pairs in MgO, CaO, SrO, and BaO ($Xe_{cation}{:}V_O$) and nearest-neighbor divacancies and Schottky trivacancies in hafnia ($Xe_{Hf}{:}V_O$, $Xe_{Hf}{:}2V_O$). Results from variable charge model are given. Results from the charge compensation model (where charge states differ in calculations) are in parentheses. All divacancy results are indicated in bold.

Oxide	Defect	Incorporation energy (eV)	Charge state
MgO	$Xe_{Mg}{:}V_O$	**5.2**	0
	Xe_{Mg}	8.1 (12.4)	0 (−2)
	Xe_O	8.3	+2
	I_{Xe}	18.7	0
CaO	$Xe_{Ca}{:}V_O$	**2.1**	0
	I_{Xe}	12.1	0
SrO	$Xe_{Sr}{:}V_O$	**1.3**	0
	I_{Xe}	9.5	0
BaO	$Xe_{Ba}{:}V_O$	**0.8**	0
	I_{Xe}	6.7	0
HfO_2	$Xe_{Hf}{:}V_O$	**3.9 (5.4)**	0 (−2)
	$Xe_{Hf}{:}2V_O$	2.7	0
	Xe_{Hf}	2.9 (9.1)	0 (−4)
	Xe_O	11.0	+2
	I_{Xe}	16.5	0

In the case of HfO_2, also shown in table 3, the Xe incorporation energies at different Hf defect sites are all similar, regardless of the local oxygen vacancy configuration: Xe_{Hf}^0, 2.9 eV, $(Xe_{Hf}{:}V_O)^0$, 3.9 eV, and $(Xe_{Hf}{:}2V_O)^0$, 2.7 eV. On the other hand, the Xe incorporation energies at interstitial or oxygen vacancy site are quite high. In figure 1, we plot the DFT results for Xe incorporation energy as a function of cation radii in alkaline earth metal oxides (Mg^{2+}, 0.57 Å, Ca^{2+}, 1.0 Å, Sr^{2+}, 1.18 Å, Ba^{2+}, 1.35 Å), and compare with that in HfO_2. Only the Xe incorporation energies at divacancy and interstitial sites are plotted. All substitutional incorporation energies are lower than the interstitial case, which means it is less likely for Xe to be incorporated into an interstitial site. As seen in figure 1, comparing the incorporation of Xe to the equivalent case of Xe in the divacancy site in hafnia shows that the energy required to incorporate Xe in hafnia is 1.3 eV less than in MgO[1]. However, as cation size of the alkaline earth

[1] We did the comparison to the divacancy case in hafnia here based on consideration of the similar stoichiometry of the fission product containing clusters in MgO.

Table 4. Cs and Sr incorporation energies in bulk oxides: nearest-neighbor Schottky pair in MgO, CaO, SrO, and BaO (Cs_{cation}:V_O), divacancy and trivacancy in hafnia (Cs (or Sr)$_{Hf}$:V_O, Cs_{Hf}:$2V_O$), and cation vacancies (Cs (or Sr)$_{cation}$). Results from the charge compensation model (where charge states differ in calculations) are in parentheses. Divacancy results of Cs incorporation are indicated in bold. In some cases, although the charge states of fission product defects in the two models are the same, the incorporation energy may be different, since the reference defect is in a different charge state.

Oxide	Cs defects	Incorp. energy (eV)	Charge state	Sr defects	Incorp. energy (eV)	Charge state
MgO	Cs_{Mg}:V_O	**0.4**	+1	Sr_{Mg}	−7.2 (−7.7)	0 (0)
	Cs_{Mg}	3.1 (4.0)	0 (−1)			
CaO	Cs_{Ca}:V_O	**−2.2**	+1	Sr_{Ca}	−9.2 (−9.5)	0 (0)
SrO	Cs_{Sr}:V_O	**−2.8**	+1	Sr_{Sr}	−9.2 (−9.4)	0 (0)
BaO	Cs_{Ba}:V_O	**−2.8**	+1	Sr_{Ba}	−8.2 (−8.2)	0 (0)
HfO_2	Cs_{Hf}:V_O	**−1.5** (**−1.5**)	0 (−1)	Sr_{Hf}	−10.1 (−10.3)	0 (−2)
	Cs_{Hf}:$2V_O$	−2.7	+1	Sr_{Hf}:V_O	−9.7	0
	Cs_{Hf}	−0.8 (0.7)	0 (−3)			

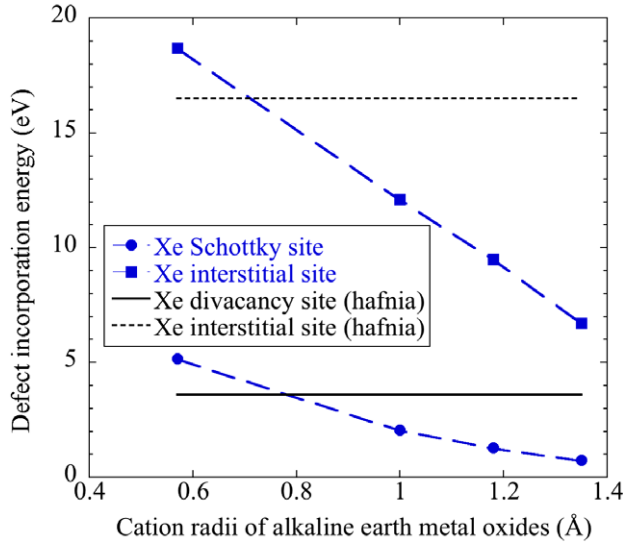

Figure 1. Xe incorporation energies in MgO, CaO, SrO, and BaO as a function of cation radii. Filled circles are energies for Xe incorporation into Schottky defect sites and filled squares are in interstitial sites. Corresponding results in hafnia are the solid (divacancy site) and dotted (interstitial site) lines. For hafnia, the lines are plotted merely as guides for the eye. There are no alkaline earth cations in hafnia; hence, there is no dependences on cation radius.

metal oxide increases, this trend reverses. In fact, for all other alkaline earth metal oxides, the incorporation energy of Xe is lower than it is for hafnia.

In table 4, we show similar results for the incorporation of Cs and Sr in alkaline earth metal oxides. In the case of Cs, the trends are very similar to Xe. The primary difference is that the incorporation energies are now negative in most oxides. For Cs substitution in alkaline earth metal oxides, take MgO as an example, there are three possible incorporation sites: substitution on the Mg vacancy site, Cs_{Mg}; substitution on the Schottky divacancy site, (Cs_{Mg}:V_O); and the formation of a cluster (Cs_{Mg}:V_O:Cs_{Mg}) containing two Cs atoms [6]. In MgO, the incorporation energy for Cs_{Mg} is 2.7 eV higher than that for (Cs_{Mg}:V_O). The formation of the cluster geometry (Cs_{Mg}:V_O:Cs_{Mg}) requires a second Cs_{Mg}, and we will consider this later (see below). In table 4, comparison with the equivalent case of Cs in the divacancy site in hafnia shows that the energy required to incorporate Cs in such a site is 1.9 eV less than in MgO. However, as cation size in alkaline metal oxides increases, the trend again reverses. The Cs incorporation energies at different Hf defect sites in hafnia also show a clear trend with available defect site volume: Cs^0_{Hf}, −0.8 eV; $(Cs_{Hf}:V_O)^0$, −1.5 eV; and $(Cs_{Hf}:2V_O)^+$, −2.7 eV (see table 4).

The above cases only apply for Cs solution in oxides. We have also carried out DFT calculations of Cs_2O precipitation in MgO. The Cs_2O bulk in our DFT calculations is in $CdCl_2$ crystal structure, which is characterized by an AbC BcA CaB stacking sequence of Cs and O layers [21]. Specifically, three reactions were considered:

$$2MgO + 2Cs_{Mg} + V_O \rightarrow Cs_2O + 2Mg_{Mg} + O_O \quad (3)$$

$$2MgO + Cs_{Mg} + (Cs_{Mg}:V_O) \rightarrow Cs_2O + 2Mg_{Mg} + O_O \quad (4)$$

$$2MgO + (Cs_{Mg}:V_O:Cs_{Mg}) \rightarrow Cs_2O + 2Mg_{Mg} + O_O. \quad (5)$$

Each of the above sets of reactions (equations (3)–(5)) is exothermic (heat is released), with DFT reaction enthalpies of-19.4 eV (equation (3)), −14.7 eV (equation (4)), and −12.5 eV (equation (5)). If the charge compensation model is used, the reaction enthalpies are −22.2 eV (equation (3)), −16.2 eV (equation (4)), and −12.5 eV (equation (5)). The differences in the calculated enthalpies reflect the binding energies of the (Cs_{Mg}:V_O) (4.7 eV) and (Cs_{Mg}:V_O:Cs_{Mg}) cluster (2.2 eV) respectively. Since the reaction enthalpies are quite large, Cs solution in MgO should then only occur in the dilute limit. We also computed the reaction enthalpies for the last reaction (similar to equation (5)) in other alkaline earth metal oxides. The calculated results are −5.2 eV (CaO), −3.2 eV (SrO), −1.5 eV (BaO). The DFT results show that the precipitation tendency is greatly reduced in oxides with larger cation sizes.

For Sr substitution in alkaline earth metal oxides, since Sr is a +2 ion, with a charge state equal to that of the cation in these oxides, we simply substitute Sr on cation vacancy sites and assume this is the most favorable incorporation site. The DFT results for Sr incorporation energies are also listed in table 4. From table 4, we note an initial reduction in Sr incorporation energies (1–2 eV) when the cation size increases. However, for BaO, it increases again, indicating a non-monotonic behavior with cation radius. The incorporation energies of Sr in alkaline earth metal oxides are generally large

(negative). This is due to the strong bonding energy of Sr–O in these oxides. For example, the cohesive energy of SrO is about −10.7 eV per Sr–O pair in our calculations (with spin-polarized atomic contributions taken into account). The Sr incorporation in hafnia is calculated to be ∼−10 eV, for both Sr_{Hf} and (Sr_{Hf}:V_O) cases. This energy is 2.8 eV smaller than in MgO and is also smaller than for any of the alkaline earth metal oxides, meaning that Sr will prefer hafnia over any of these compounds. This is in contrast to Cs and Xe, which both prefer the larger cation radius alkaline earth oxides over hafnia.

3.2. Segregation at MgO–HfO_2 interface

In order to understand the qualitative impact of interfaces between MgO and cubic HfO_2 on fission product segregation, we use as a model structure, the structure of an MgO/cubic ZrO_2 interface from a directionally solidified eutectic, as determined by high resolution TEM [22]. This structure aligns the [211] direction of MgO with the [100] direction of hafnia, and the interface planes are $(1\bar{1}\bar{1})$ in MgO and (001) in hafnia. Similar interfacial structures for NiO–ZrO_2 have been studied [23, 24]. Bulk NiO has the same rock-salt structure as MgO. The lattice constant mismatch between NiO and ZrO_2 is 23%, which is similar to the 21% mismatch between MgO and HfO_2. So we assume that the results on the NiO–ZrO_2 interface should also apply to the MgO–HfO_2 interface. In [23], two types of ZrO_2(100)–NiO(111) interfaces were studied, (Zr–O_2)–(Ni–O) (type I) and (O_2–Zr)–(O–Ni) (type II). It was found that the type II structure is lower in energy. This structure is the same as that found for the MgO–ZrO_2 interface in [22]. In another study, Fisher and Matsubara [24] studied different possible interfaces formed between NiO and ZrO_2 using the molecular dynamics method with pair potentials. In their study, the ZrO_2(100)–NiO(111) interface was found to have lowest interfacial energy at 1273 K, although the detailed interfacial structure is different as the number of oxygen atoms at the interface was allowed to vary. The interface found has an interphase boundary of a shared oxygen plane, retaining a pseudocrystalline structure. However, because of the large periodicity in such a pseudocrystalline structure, it is computationally impractical to model or test this structure within a DFT scheme. Instead, we choose the type II structure as our model MgO–HfO_2 interface structure here.

We adopted a slab model for our MgO/HfO_2 interface calculations. In figures 2(a) and (b), the relaxed model interface structure is shown from two perspectives: [211] and $[01\bar{1}]$ directions relative to the MgO bulk. The interface structure consists of eight layers of cubic HfO_2 and 12 layers of MgO, with surface terminations. The interface structure was constrained to the lattice constants of bulk MgO in appropriate directions and cubic HfO_2 layers were strained accordingly in interfacial dimensions. After the interface model was constructed, full relaxations of atomic positions were carried out. During the relaxations, the top five HfO_2 layers were fixed to mimic the bulk HfO_2 structure. The interface structure in the simulations contains 120 atoms. Bigger slab models are desired to understand possible size effect and associated structural variations, however, cells containing

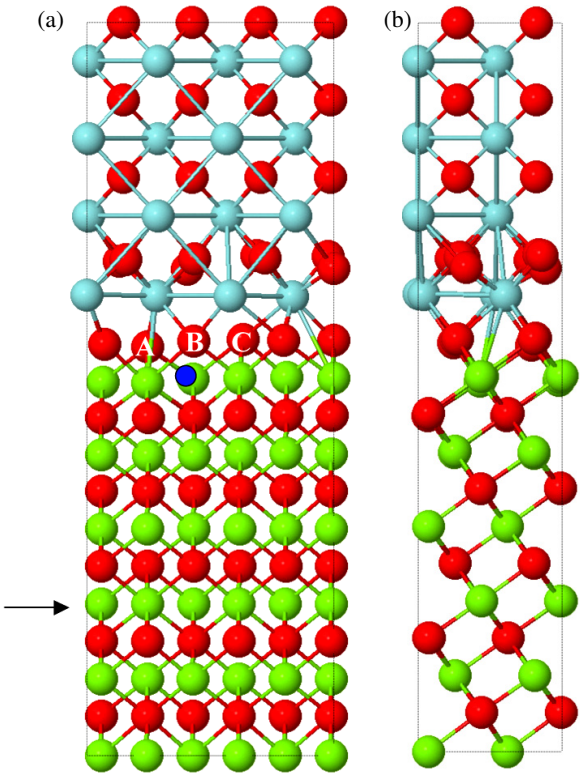

Figure 2. (Color online) MgO–HfO_2 interface model. (a), (b) Final relaxed interface structure, viewed from (a) the [211] direction, (b) the $[01\bar{1}]$ direction, with respect to the MgO side of the interface. In the figure, red spheres are oxygen, green are Mg, and light-blue are Hf. For the interface region, in the case of fission product substitution in the divacancy Schottky site, three possible locations of the oxygen vacancy site are labeled as A, B, C (in (a) only). The corresponding cation substitution position for the fission product atom is marked by the small dark-blue sphere. The bulk location of Mg site is indicated by an arrow.

120 atoms, including transition metal elements, are already very computationally demanding with current computational resources and larger sizes are prohibitive.

Segregation studies were performed on the resulting relaxed interface structure. Each fission product and its associated defect structure were incorporated in the MgO side of the interface, and the total energy of the structure after relaxation was obtained. Sensitivity tests on the bulk-like region in the 3rd or 4th layer from the interface reveal a difference in total energies of less than 0.05 eV. We thus choose the bulk location as the Mg site in the 4th layer from interface (3rd layer from bottom MgO surface). For the interface region, in the case of fission product substitution in the divacancy Schottky site, there are three possible locations of the oxygen vacancy site (see figure 2(a), labeled as A, B, C). In this case, three sets of interface calculations were carried out and the total energy of each structure after relaxation was obtained. The energy difference of the fission product substitution at the interface versus within the MgO bulk-like region defines the segregation enthalpy at interface.

The results for segregation enthalpies for Xe, Cs, and Sr are summarized in table 5. For Xe substitution at a divacancy Schottky site, the segregation enthalpy to the interface ranges

Table 5. DFT segregation enthalpies for Xe, Cs, and Sr at model $MgO–HfO_2$ interface.

	Oxygen vacancy site	$H_{seg.}$ (eV)
$(Xe_{Mg}:V_O)^0$	A	−3.0
	B	−1.9
	C	−1.8
$(Cs_{Mg}:V_O)^+$	A	−3.3
	B	−3.0
	C	−2.4
Sr^0_{Mg}	—	−1.0

from −1.8 to −3.0 eV. For Cs, substitution at the divacancy Schottky site has an interfacial segregation enthalpy of −2.4 to −3.3 eV. Finally, for Sr, simple substitution for a Mg cation has an interfacial segregation enthalpy of −1.0 eV.

The DFT calculation results reflect our attempt to understand the segregation behavior between different bulk phases and the interface between the matrix and fuel core material in a possible dispersion fuel form, as stated in the introduction part. For a surrogate material HfO_2 in replacement of UO_2, and inert matrix such as MgO, our calculations show that for the three fission products Xe, Cs, and Sr, the fission products prefer to reside in HfO_2 over MgO. And these fission products could also readily segregate to the interfaces. These results suggest that the inert matrix material selection of MgO is not optimal. Other alkaline earth metal oxides with larger cation size should also be considered. However, other important factors have not yet been considered, including the role of microstructure such as grain-boundaries, and the role of kinetics during the collision cascade when the fission product is produced. These two factors, to be investigated in the near future, might make substantial contributions to the possible physical processes considered here.

4. Summary

DFT calculations of fission product (Xe, Cs, and Sr) incorporation into alkaline earth metal oxides (MgO, CaO, SrO, and BaO) and hafnia, as well as possible segregation behavior at a model $MgO–HfO_2$ interface, were carried out. From studying defects in MgO, we found that the charge compensation model in general yields better energetic results than neutral calculations. However, in certain cases, an approach using the variable charge model needs to be considered to account for electronic structure effects. We also found that the fission product incorporation energy is smaller in hafnia than in MgO for Cs and Sr, and Xe if a variation of charge state is allowed. This trend in incorporation energy is reversed or reduced for alkaline earth metal oxides with larger cation sizes. Calculations of the segregation enthalpy at a model $MgO–HfO_2$ interface revealed strong segregation tendencies from MgO bulk to $MgO–HfO_2$ interfaces for all three dopant elements considered.

Acknowledgments

We thank Chris Stanek and Steve Valone for many stimulating discussions. This work was supported by the Los Alamos National Laboratory Directed Research and Development Program. LANL is operated by Los Alamos National Security, LLC, for the National Nuclear Security Administration of the US Department of Energy under Contract No. DE-AC52-06NA25396.

References

[1] Crocombette J-P 2002 *J. Nucl. Mater.* **305** 29
[2] Peacock P W, Xiong K, Tse K and Robertson J 2006 *Phys. Rev.* B **73** 075328
[3] Du Z, Allan N L, Blundy J D, Purton J A and Brooker R A 2008 *Geochim. Cosmochim. Acta* **72** 554
[4] Kresse G and Hafner J 1993 *Phys. Rev.* B **47** 558
Kresse G and Furthmüller J 1996 *J. Comput. Mater. Sci.* **6** 15
[5] Henkelman G, Uberuaga B P, Harris D J, Harding J H and Allan N L 2005 *Phys. Rev.* B **72** 115437
[6] Vyas S, Grimes R W, Binks D J and Rey F 1997 *J. Phys. Chem. Solids* **58** 1619
[7] Foster A S, Lopez Gejo F, Shluger A L and Nieminen R M 2002 *Phys. Rev.* B **65** 174117
[8] De Vita A, Gillan M J, Lin J S, Payne M C, Stich I and Clarke L J 1992 *Phys. Rev. Lett.* **68** 3319
[9] De Vita A, Gillan M J, Lin J S, Payne M C, Stich I and Clarke L J 1992 *Phys. Rev.* B **46** 12964
[10] Alfe D and Gillan M J 2005 *Phys. Rev.* B **71** 220101(R)
[11] Gilbert C A, Kenny S D, Smith R and Sanville E 2007 *Phys. Rev.* B **76** 184103
[12] Leslie M and Gillan M J 1985 *J. Phys. C: Solid State Phys.* **18** 973
[13] Wyckoff R W G 1964 *Crystal Structures* (New York: Wiley)
[14] Sangster M J L, Peckham G and Saunderson D H 1970 *J. Phys. C: Solid State Phys.* **3** 1026
[15] Yamashita J and Asano S 1983 *J. Phys. Soc. Japan* **52** 3506
[16] Liu L G and Bassett W A 1972 *J. Geophys. Res.* **77** 4934
[17] Chang Z P and Graham E K 1977 *J. Phys. Chem. Solids* **38** 1355
[18] Herzberg G 1952 *Can. J. Phys.* **30** 185
[19] Geng H Y, Chen Y, Kaneta Y, Iwasawa M, Ohnuma T and Kinoshita M 2008 *Phys. Rev.* B **77** 104120
[20] Henkelman G, Arnaldsson A and Jónsson H 2006 *Comput. Mater. Sci.* **36** 254
[21] Gemming S, Seifert G, Muḧle C, Jansenb M, Albu-Yaron A, Arad T and Tenne R 2005 *J. Solid State Chem.* **178** 1190
[22] Echigoya J 2005 *J. Eur. Ceram. Soc.* **25** 1381
[23] Guo C-X, Warschkow O, Ellis D E, Dravid V P and Dickey E C 2001 *J. Am. Ceram. Soc.* **84** 2677
[24] Fisher C A and Matsubara H 2005 *Phil. Mag.* **85** 1067